Journal of The Electrochemical Society

OPEN ACCESS

Structural and Magnetic Characteristics of Hematite and Magnetite Films Prepared by Electrodeposition and Heating

To cite this article: Daichi Katsuma *et al* 2022 *J. Electrochem. Soc.* **169** 042501

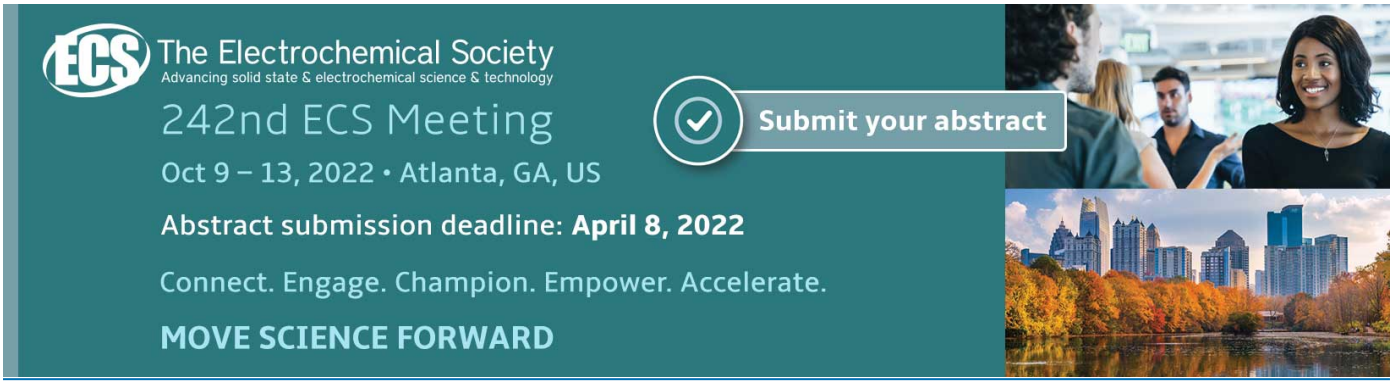

Journal of The Electrochemical Society, 2022 **169** 042501

Structural and Magnetic Characteristics of Hematite and Magnetite Films Prepared by Electrodeposition and Heating

Daichi Katsuma,[1] Pei Loon Khoo,[1,*,z] Masakazu Kobayashi,[1] Tsutomu Shinagawa,[1,2] and Masanobu Izaki[1,*]

[1]*Graduate School of Engineering, Toyohashi University of Technology, Tempaku-cho, Toyohashi-shi, Aichi 441-8580, Japan*
[2]*Electronic Materials Research Division, Morinomiya Center, Osaka Research Institute of Industrial Science and Technology, Osaka 536-8553, Japan*

Hematite (α-Fe_2O_3) films were prepared by cathodic polarization in an aqueous solution containing iron (II) sulfate hydrate, potassium hydroxide, dimethylamine-borane (DMAB), and L-ascorbic acid and their structural and magnetic characteristics were investigated with X-ray diffraction, X-ray photoelectron spectroscopy, Raman spectroscopy, scanning electron microscope observation, optical absorption measurement, and vibrating sample magnetometer (VSM), in addition to electrochemical characterizations for the electrodeposition before and after heating in ambient atmosphere and vacuum. The hematite films prepared at −1.0 and −1.1 V possessed characteristic hexagonal lattice and bandgap energy around 2.2 eV, and some amount of Fe^{2+} was contained in the hematite film, with increased Fe^{2+} content at −1.0 V. The films prepared at −0.8 and −0.9 V showed characteristic hematite bandgap energies with a decreased absorption but did not show any structural characteristics from the XRD and Raman spectra. The hematite films prepared at −1.0 V, and −1.1 V showed ferromagnetic features with 11 $A{\cdot}m^2{\cdot}kg^{-1}$ and 2.3 $A{\cdot}m^2{\cdot}kg^{-1}$ in saturation mass magnetization and 29.5, and 25 mT in coercivity, respectively. The hematite film was thermally transformed to magnetite (Fe_3O_4) possessing characteristic cubic lattice by heating at 673 K in vacuum, and the saturation mass magnetization increased to 89.2 $A{\cdot}m^2{\cdot}kg^{-1}$.
 [DOI: 10.1149/1945-7111/ac6247]

Manuscript submitted January 10, 2022; revised manuscript received February 28, 2022. Published April 6, 2022.

There are several types of iron oxides with different oxidation numbers and coordination structures,[1] with the iron oxides of α-Fe_2O_3 (Hematite), γ-Fe_2O_3 (maghemite), and Fe_3O_4 (magnetite) attracting increasing attention in chemical, medical, and electronic industries for applications such as catalysts, photoanodes, drug delivery, sensors, and magnetic devices[2] due to their low-cost abundant resources, non-toxicity, and chemical and magnetic properties. Iron oxides have been used in bulk and film shapes depending on the applications, and the iron oxide films have been prepared by vacuum processes of chemical vapor deposition,[3] evaporation,[4] and sputtering,[5] and by solution chemical processes of the sol-gel method,[6] chemical,[7] and electrochemical process.[8] Electrochemical processes including electrodeposition are favored as they possess several advantages over other preparation techniques such as the vacuum process, as demonstrated in the preparation of precursors for CIGS and CZTS solar cells.[9,10]

Direct preparations of metal oxide films by electrochemical reactions[11] have been demonstrated for ZnO,[12] Cu_2O,[13] CuO,[14] and CeO_2.[15] The magnetite (Fe_3O_4) and ferrite films were prepared directly by electrochemical[16,17] and chemical reactions[8,18] using aqueous solutions. The preparation of magnetite and zinc-ferrite films with characteristic magnetic property by electrochemical reactions in an aqueous solution containing iron (III) nitrate hydrate and dimethylamine-borane and the tentative reaction solutions have been previously reported.[8,19] However, preparations of hematite and maghemite (Fe_2O_3) have required post-heating treatments after the preparation of precursor by an electrochemical process,[20–22] and there has been great interest in a direct preparation of hematite (α-Fe_2O_3) by low-cost, facile electrochemical means.

Here, we report the direct preparation of the hematite (α-Fe_2O_3) film by electrochemical reaction from an aqueous solution containing iron (II) sulfate hydrate, potassium hydroxide, dimethylamine-borane (DMAB), and L-ascorbic acid, and the effects of the post-heating on the structural and magnetic characteristics were investigated with X-ray diffraction, X-ray photoelectron spectroscopy, Raman spectroscopy, scanning electron microscope observation, optical absorption measurement, and vibrating sample magnetometer (VSM), in addition to electrochemical characterization for electrodeposition. The hematite (α-Fe_2O_3) films prepared by electrochemical reactions revealed a ferromagnetic feature with the saturation magnetization of 11 $A{\cdot}m^2{\cdot}kg^{-1}$, and the saturation magnetization increased to 89.3 $A{\cdot}m^2{\cdot}kg^{-1}$ by heating, because of the formation of magnetite (Fe_3O_4).

Experimental

Iron oxide films were prepared on a Ga: ZnO (GZO)/SLG substrates by electrodeposition in an aqueous solution containing 0.05 mol l^{-1} of iron(II) sulfate hydrate ($FeSO_4{\cdot}7H_2O$, Kanto Chemical Co.), 0.01 mol l^{-1} of potassium nitrate (KNO_3, Kanto Chemical Co.), 0.05 mol l^{-1} of dimethylamine-borane (DMAB) ($(CH_3)_2NH{\cdot}BH_3$, Wako Pure Chemical Industries, Ltd.), and 0.2 g l^{-1} of L-Ascorbic Acid ($C_6H_8O_6$ Kanto Chemical Co.) at 313 K. The DMAB and L-ascorbic acid were added as a reducing agent as reported.[23] The electrodepositions were performed potentiostatically at −0.8, −0.9, −1.0, and −1.1 V referenced to an Ag/AgCl electrode for a constant electric charge of 1 $C{\cdot}cm^{-2}$ with a potentiostat/galvanostat (Hokuto Denko HA-501) connected to a coulombmeter (Hokuto Denko HF-201). Prior to the electrodeposition, substrates were degreased by anodic polarization at 0.2 $mA{\cdot}cm^{-2}$ for 1 min in a 0.1 mol l^{-1} sodium hydroxide aqueous solution. The counter electrode used was a Pt sheet.

The cyclic voltammogram curve (CV) was recorded at a potential range from the immersion potential of 0 to −1.5 V at a scanning rate of 10 mV s^{-1} using an automatic polarization system (HSV-110, Hokuto Denko Co., Ltd.). The Fe content in the deposited film was estimated by measuring the Fe content in the sample solution using inductively coupled plasma—optical emission spectroscopy (ICP-OES, ThermoFisher iCAP7000), which sample solution was prepared by dissolving the films in HNO_3 aqueous solution. The electron spectra were recorded using X-ray photoelectron spectroscopy (XPS, Ulvac-Phi SXM-CI) with monochromated Al kα radiation, and the spectra were corrected by referencing the adventitious carbon C1s peak at 284.6 eV. Ar sputtering was carried out under the condition of 1 kV, 1 × 1 mm^2, for 0.17 min. The X-ray diffraction patterns were recorded by out-of-plane X-ray diffraction

*Electrochemical Society Member.
[z]E-mail: khoo@me.tut.ac.jp

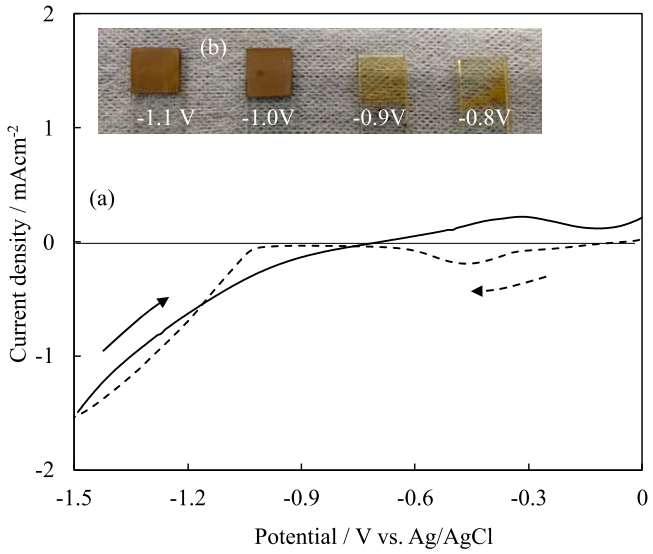

Figure 1. Cyclic voltammogram (a) for the cathodic polarization in aqueous solution containing iron (II) sulfate hydrate, potassium nitrate, L-ascorbic acid, and dimethylamine-borane, and appearance of the films deposited at −0.8 V, −0.9 V, −1.0 V, and −1.1 V (b).

using Rigaku RINT 2500 with monochromated CuKα radiation operated at 40 kV and 200 mA, and Grazing Incidence X-ray diffraction (GI-XRD) at fixed incident angles of 0.5 and 1.0 degrees using Rigaku SmartLab with monochromated CuKα radiation operated at 40 kV and 150 mA. The Raman spectra were recorded using Horiba LabRAM HR Evolution with a CO_2 laser at a wavelength of 532 nm. The Fourier transform infrared (FT-IR) spectra were recorded using Jasco 6300 type A with a diamond ATR. The surface and cross-sectional morphologies were observed using field-emission scanning electron microscopy (FE-SEM, Hitachi SU-5000). The optical absorption spectra were recorded by UV–vis-NIR spectroscopy (HITACHI-Hightech, UV-4100) referenced to a bare GZO/SLG substrate. The magnetic hysteresis curves were recorded with a vibrating sample magnetometer (VSM, Riken Denshi, BHV-50H) at room temperature.

Results and Discussion

Structural and magnetic characteristics for hematite films prepared by electrodeposition.—Figure 1 shows the cyclic voltammogram curve recorded by scanning the immersion potential from 0 to −1.5 V and back for the electrodeposition. The appearance of the solution remained clear and colorless before and after the measurement, with no formation of precipitation observed in the solution. When scanned in the direction from the immersion potential of 0 V, the cathodic current density started increasing gradually from −0.08 V, which decreased towards −0.6 V after reaching a small peak at −0.45 V, which then increased rapidly again from −1.0 V.

The electrodeposition of oxide in an aqueous solution containing nitrate ions can be generated by reduction of the nitrate ions with the formation of hydroxide ions in the vicinity of the cathode substrate as follows[11]:

$$NO_3^- + H_2O + 2e^- \rightleftarrows NO_2^- + 2OH^-$$
$$E^0 = 0.01 \text{ V vs SHE}$$

and the equilibrium potential for the Fe^{2+}/Fe^0 oxidation-reduction reaction can be expressed as follows[24]:

$$Fe^{2+} + 2e^- \rightleftarrows Fe^0 \quad E = -0.440 + 0.0295 \log [Fe^{2+}](\text{V vs SHE})$$

When the dissolved species of *Fe* were to mainly consist of Fe^{2+} ions in the solution, the potential (*E*) was estimated to be −0.68 V (Ag/AgCl).

The potential around −0.4 V for the small current density peak was more negative than the NO_3^-/NO_2^- reaction potential and more positive than the Fe^{2+}/Fe^0 reaction potential, suggesting that the current density around −0.4 V originated from the NO_3^-/NO_2^- reaction. The depositions of iron oxide or iron hydroxide at potentials more negative than −0.2 V were also possible.

In the return scan from −1.5 V, the cathodic current density linearly decreased when the potential was brought towards the positive side and reached the current density of 0 mA cm^{-2} at approximately −0.6 V, which was close to the equilibrium potential for the Fe^{2+}/Fe^0 reaction, indicating the formation of metallic Fe by cathodic polarization at the potential of −1.5 V. And the increase in the cathodic current density from approximately −1.1 V in the

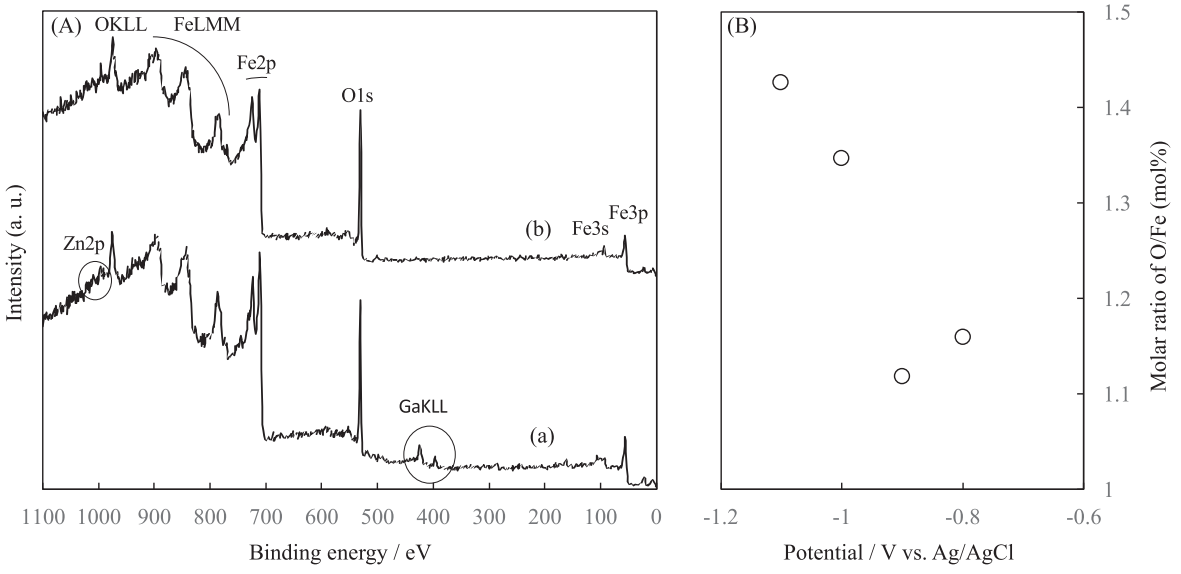

Figure 2. Photoelectron spectra (A) for films deposited at −0.9 (a), and −1.0 V (b) vs Ag/AgCl, and the effect of potential on the molar content of Fe and O elements (B).

forward scanning originated from the reduction reaction to metallic Fe from the iron oxide or hydroxide deposited at potentials negative than −0.2 V. As such, to investigate the electrodeposition of oxide, the voltage must be below the estimated theoretical value of −0.68 V as aforementioned, but higher than −1.5 V to avoid the formation of metallic Fe. Thus, the iron oxide or hydroxide films were prepared at potentials of −0.8, −0.9, −1.0, and −1.1 V for 1 C·cm^{-2}, and their appearances are shown in Fig. 1b. The films prepared at −0.8 and −0.9 V appeared brownish while −1.0 and −1.1 V appeared yellowish, which resembled Fe_2O_3 and FeOOH respectively, and not Fe_3O_4 which is black in color.

Figure 2 shows the electron spectra recorded at binding energy ranging from 1100 to 0 eV for the films prepared at −0.9 and −1.0 V, and the relationship of molar concentration ratio of Oxygen to Fe elements (O/Fe ratio) depending on the deposition potential. The electron spectra for −0.9 and −0.8 V were almost the same in profile and peak energies, while −1.0 V was similar to that of −1.1 V. All the peaks observed for the film prepared at −1.0 V were identified as peaks originating from Fe and O elements, while additional peaks at 162 eV, 395 ∼ 422 eV, and 1006 ∼ 1020 eV,[25] were observed for the film prepared at −0.9 V in addition to the peaks of Fe, and O elements. These additional peaks could be assigned to Ga and Zn elements. Since Ga: ZnO-coated SLG glass was used as the substrates, the presence of Ga and Zn elements originating from the substrate indicated that the deposited films did not entirely cover the surface of the substrates. The binding energies for the $Fe2p_{3/2}$ peaks were estimated to be 709.5, 709.5, 710.6, and 710.9 eV at −0.8, −0.9, −1.0, and −1.1 V from the Fe2p narrow spectra (not shown), respectively. The reported values of the binding energies for the $Fe2p_{3/2}$ peaks were 710.9, 710.6, and 709.9 eV for Fe_2O_3, Fe_3O_4, and FeO, respectively.[26,27] The binding energies of $Fe2p_{3/2}$ peaks for the films deposited at −0.8, and −0.9 V were close to that of FeO, and the binding energies for −1.0 and −1.1 V were close to those of Fe_3O_4 and Fe_2O_3, respectively. The values of the binding energies indicated that the Fe element in the deposited films mainly existed as Fe^{2+} state in the films prepared at −0.8 and −0.9 V and as a mixture of Fe^{2+} and Fe^{3+} states (mainly Fe^{3+}) in the films prepared at −1.0 and −1.1 V.

The O/Fe ratios shown in Fig. 2B were estimated from the Fe2p and O1s photoelectron peaks using tabulated sensitivity factors (at a mounting angle of 45°).[28] The films prepared at −0.8 and −0.9 V showed O/Fe ratios of 1.12 ∼ 1.16, which increased when the potential was brought towards the negative side. The O/Fe stoichiometric composition ratios were 1.5, 1.33, and 1 for Fe_2O_3, Fe_3O_4, and FeO respectively. Considering this, while the O/Fe ratios calculated from the photoelectron peaks contained some degree of uncertainty, the O/Fe ratio for the films prepared at −1.0 and −1.1 V were close to those of Fe_3O_4 and Fe_2O_3, and the ratios at −0.8 V, and −0.9 V were close to that of FeO.

Figure 3 shows the grazing-incident X-ray diffraction (GI-XRD) patterns and the Raman spectra for the iron oxide films prepared at −0.8, −0.9, −1.0, and −1.1 V. As references, the Raman spectra for the α-Fe_2O_3 and Fe_3O_4 standard powders were also shown in Fig. 3b. The GI-XRD technique at a fixed incident angle of 1.0 degrees was deployed since no diffracted X-ray peak could be observed when measured with the conventional $\theta/2\theta$ scanning technique. A diffracted X-ray peak originating from ZnO with the characteristic wurtzite lattice in the GZO/SLG substrate could be observed for all the X-ray diffraction patterns at 34.5 degrees. Additionally, two peaks were observed at 26.3 and 35.6 degrees for the iron-oxide films prepared at −1.0 and −1.1 V, and these two peaks could be assigned as the (012) and (110) plane for hematite (α-Fe_2O_3) with a characteristic hexagonal lattice.[29] On the other hand, no such additional peaks could be observed for the iron-oxide films prepared at −0.8 and −0.9 V. This may have been due to the small thicknesses of the layers, as seen as partly transparent from the appearance photo as shown in Fig. 1.

From the Raman spectra shown in Fig. 3b, five peaks were clearly observed at wavenumbers of 216, 279, 391, 592, and 1285 cm^{-1}, and these peaks could be assigned as A_{1g}, E_{1g}, and $2E_u$ vibrations for the hematite (α-Fe_2O_3) by comparing to those of an α-Fe_2O_3 powder standard, although there were slight differences in relative intensities among them.[30] The peak shoulder located at the long wavenumber side of the α-Fe_2O_3 E_{1g} peak, as represented by an arrow, was observed for the spectra of −1.0 and −1.1 V with its wavenumber close to a Fe_3O_4 peak, suggesting the existence of small amounts of Fe_3O_4 in the hematite films. Also, no stretching vibration of OH^- in the form of H_2O at around 3300 cm^{-1} could be observed from the FT-IR spectra (not shown), ruling out inclusion of OH^- for the iron-oxide films prepared at −1.0 and −1.1 V.[31] From the X-ray diffraction patterns, Raman spectra, and FT-IR spectra, the iron oxide films prepared at −1.0 and −1.1 V could be identified as hematite (α-Fe_2O_3), with the possibility of containing some amount of Fe^{2+} species according to the binding energy of Fe2p electron peaks shown in Fig. 2.

The iron oxide films prepared at −0.8 and −0.9 V possessed no clear peaks identified as Fe_2O_3, Fe_3O_4, and FeO on the Raman spectra. The FT-IR spectra were different in profile to those at −1.0 and −1.1 V, and absorption band at 896 and 760 cm^{-1}, which could be identified as those for Fe-OH vibration, were observed for the FT-IR spectra (not shown), although there was no absorption band around 3300 cm^{-1}.[31–33] There was a possibility of the inclusion of Fe-OH component in the iron-oxide films from the IR absorption spectra.

Figure 4 shows the optical transmission spectra for iron oxide films prepared at −0.8, −0.9, −1.0, and −1.1 V. Also shown are the relationships between the optical absorption coefficient and the photon energy for the iron-oxide films prepared at −0.9 and −1.0 V with the assumption of indirect and direct transitions. The absorption coefficients were estimated from the absorbance of the optical absorption spectra and thicknesses calculated from the Fe content analyzed with ICP-OES. The Fe content in the films was quantitatively estimated with ICP-OES. The thickness of the hematite films was obtained by assuming that hematite (α-Fe_2O_3) possesses a density of 5.2 g·cm^{-3}.

The iron oxide films prepared at −0.8 and −0.9 V showed high optical transparencies over 80% in transmission at wavelengths above 500 nm, and small absorption edges were observed at around 500 nm of the transmission curves. The transmission decreased with the decrease in wavelength from below approximately 500 nm, but the minimum value observed around 340 nm did not reach 0%, indicating insufficient coverage of the films over the entire substrate surface. The Ga and Zn elements originating from the GZO/SLG substrate were detected by XPS-analysis, and the minimum transmission above 0% was consistent with the XPS analysis results indicating exposed substrates. The hematite films prepared at −1.0 and −1.1 V showed transmissions of 20% and 32% at the wavelength of 800 nm, and the transmissions decreased with the decrease in wavelength.

The relationship between the optical absorption coefficient (α) and photon energy ($h\nu$) is as follows:

$$(\alpha h\nu)^n \propto (h\nu - E_g)$$

where E_g, h, and ν represent the bandgap energy, plank constant, and photon frequency. n = 2 and 1/2 are generally used for direct and indirect transitions.[15] The relationships for the iron-oxide films were shown in the cases of both the indirect (B) and direct transitions (C). The bandgap energies for the iron oxide film prepared at −0.9 V were roughly 2.28 and 2.25 eV when estimated for indirect and direct transitions, while the hematite film prepared at −1.0 V showed bandgap energies of 2.18 and 2.19 eV for indirect and direct transitions. It was reported that hematite (α-Fe_2O_3) possess a 2.1 ∼ 2.3 eV bandgap energy,[34] which agrees with the estimated

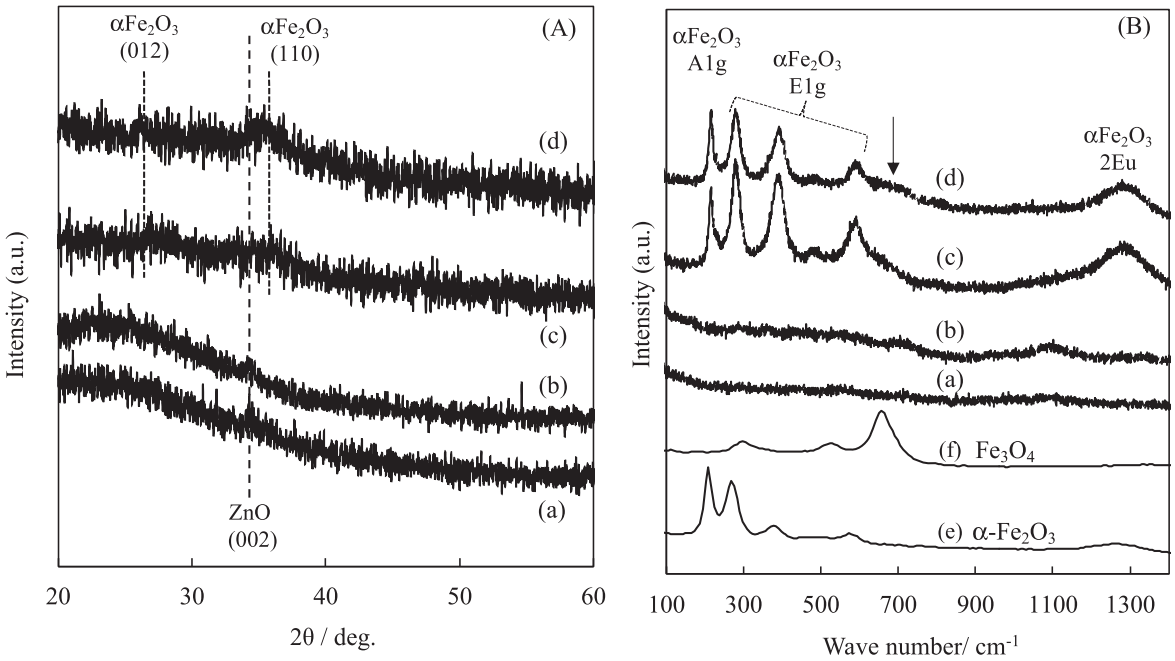

Figure 3. GI-X-ray diffraction patterns (A) and Raman spectra (B) for films deposited at −0.8 V (a), −0.9 V (b), −1.0 V (c), and −1.1 V (d) vs Ag/AgCl. Raman spectra for α-Fe_2O_3 (e) and Fe_3O_4 (f) standard powders.

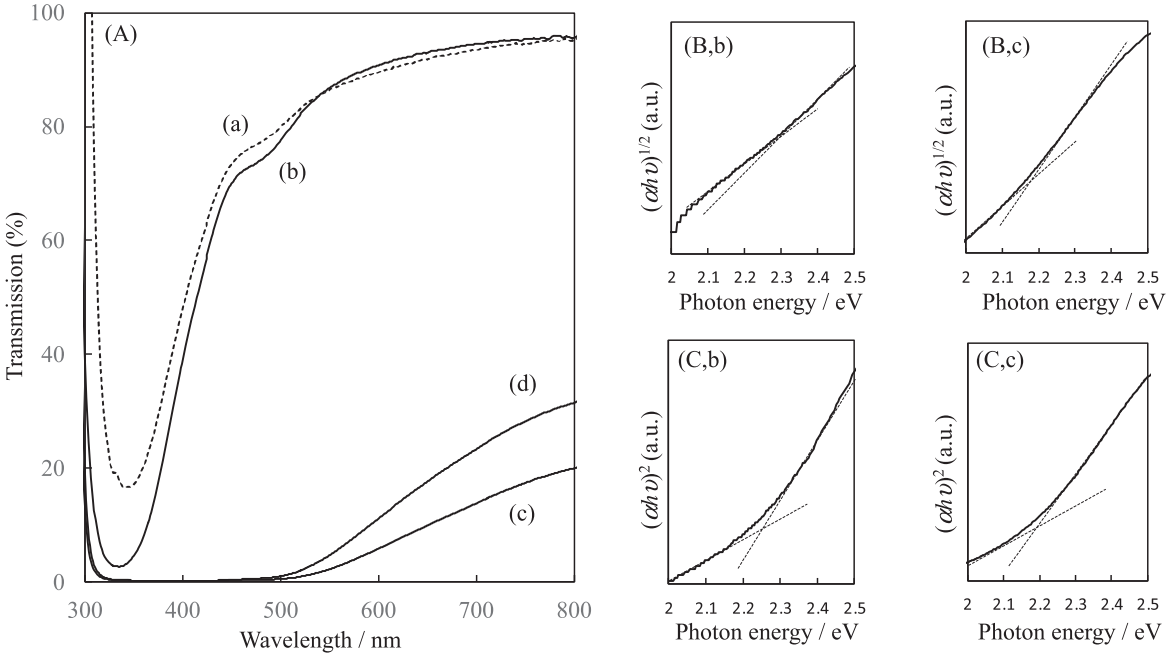

Figure 4. Optical transmission spectra (A) for films deposited at −0.8 V (a), −0.9 V (b), −1.0 V (c), and −1.1 V (d) vs Ag/AgCl, and the relationships between the absorption coefficient and photon energy for the films prepared at −0.9 V (b), and −1.0 V (c) with assumption of indirect (B) and direct (C) transitions.

bandgap energies for iron oxide films prepared at −0.9 and −1.0 V. The iron oxide films prepared at −1.0 and −1.1 V were already identified as hematite (α-Fe_2O_3) from the XRD and Raman spectra, and from the bandgap energies, the iron oxide films prepared at −0.8 and −0.9 V were also mainly composed of hematite (α-Fe_2O_3).

Figure 5 shows the surface and cross-sectional images of hematite films prepared at −0.8, −0.9, −1.0, and −1.1 V. The hematite films prepared at −0.8 and −0.9 V were composed of aggregates of fan-shaped grains and possessed rough surface irregularities. The average thicknesses estimated roughly from the cross-sectional images were approximately 1.1 and 1.4 μm at −0.8 and −0.9 V, and the values were very different from 0.40 and 0.28 μm in average thickness as estimated from the ICP-OES analysis. Since Ga and Zn elements from the GZO/SLG substrate were detected by XPS analysis, the iron-oxide films may not have covered the entire substrate surface, partially exposing the GZO/SLG substrate surface.

The hematite film prepared at −1.0 V was composed of aggregates of granular grains with 0.55 ∼ 1.2 μm in size. The surface irregularity was very large due to the coalescence of granular grains, and the hematite film was deposited over the entire substrate surface. The average thickness estimated was approximately 27.8 μm, which was also different from the 4.2 μm estimated from the ICP-OES analysis.

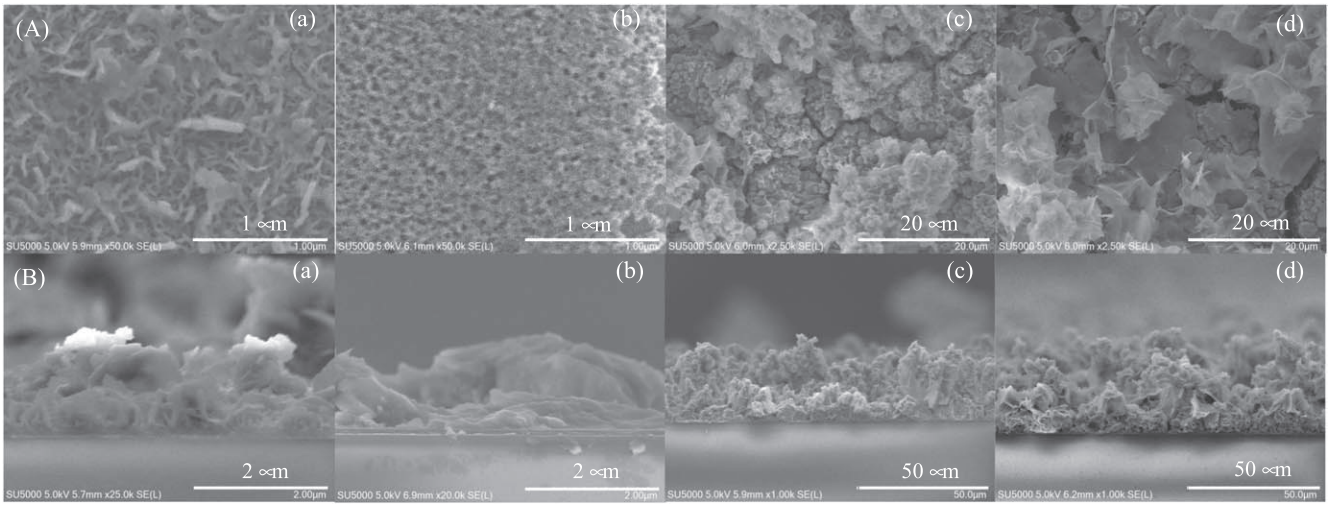

Figure 5. Surface (A) and cross-sectional images (B) for iron oxide films deposited at −0.8 V (a), −0.9 V (b), −1.0 V (c), and −1.1 V (d) vs Ag/AgCl.

The bilayer composed of upper fan-shape grain and bottom granular grain layers were observed for the hematite film prepared at −1.1 V, and the surface irregularity was extremely large, causing difficulty to estimate its thickness, but the thickness obtained with ICP-OES was 3.5 μm. While the values of the thickness estimated with the ICP-OES analysis showed a similar tendency as those estimated from the SEM image, they were largely different due to the actual large surface roughness and porous structure of the film. Since the electrodeposition was carried out at constant electric charge irrespective of the potential, it can be said that the current efficiency of the hematite electrodeposition was very different between −0.8, −0.9 V, and −1.0, −1.1 V. The amount and thickness of the hematite films estimated with the ICP-OES analysis were used for the calculation of mass magnetization in magnetic characterization.

Figure 6 shows the magnetic hysteresis curves for hematite films prepared at −0.8, −0.9, −1.0, and −1.1 V. Only two hematite films prepared at −1.0 and −1.1 V showed ferromagnetic features at room temperature. The saturation mass magnetization and coercivity were estimated to be 11.0 $A{\cdot}m^2{\cdot}kg^{-1}$, 29.5 mT, and 2.3 $A{\cdot}m^2{\cdot}kg^{-1}$, 25 mT for hematite films prepared at −1.0 and −1.1 V, respectively. It was reported that the magnetite and hematite possess a mass magnetization of ∼92 $A{\cdot}m^2{\cdot}kg^{-1}$ and ∼0.4 $A{\cdot}m^2{\cdot}kg^{-1}$ and coercivity of 10 ∼ 40 mT and ∼100 ∼ 400 mT, respectively.[1] The coercivities of 25 ∼ 29 mT for the hematite films prepared by electrodeposition were located within the range for magnetite, which is smaller than those reported for hematite. However, the saturation magnetization of 2.3 ∼ 11 $A{\cdot}m^2{\cdot}kg^{-1}$ was much smaller than that for magnetite and larger than that of hematite. The $Fe2p_{3/2}$ peaks for the hematite films prepared at −1.0 and −1.1 V indicate the existence of Fe^{2+} state from the binding energy close to that for magnetite, and also the shoulder peak from the Raman spectra indicated the existence of a small amount of magnetite (Fe_3O_4) in the hematite film. However, it was difficult to detect the X-ray diffraction peaks originating from the magnetite due to the close d-values of magnetite (312) and hematite (110) planes at around 35.6 degrees. It was speculated that the ferromagnetic feature originated from the magnetite formed in the hematite films that appeared on the magnetic hysteresis curves, and the saturation magnetization reflected the amount of magnetite embedded in the hematite films.

The tentative reaction schemes for the electrodeposition of hematite films were speculated as follows, according to the reaction schemes already reported for the electrodeposition of oxides including magnetite (Fe_3O_4). The Fe ions dissolved in the aqueous solution used for the preparation mainly existed as Fe^{2+} ions because of the existence of L-ascorbic acid and dimethylamine-borane (DMAB) as the reducing agents, with a small amount of Fe^{3+} ion as reported in Fe electroplating baths with reducing agents.[23] And the standard Gibbs free energy was obtained by the thermodynamic calculation using the chemical potential, that is standard Gibbs free energy for formation.[11]

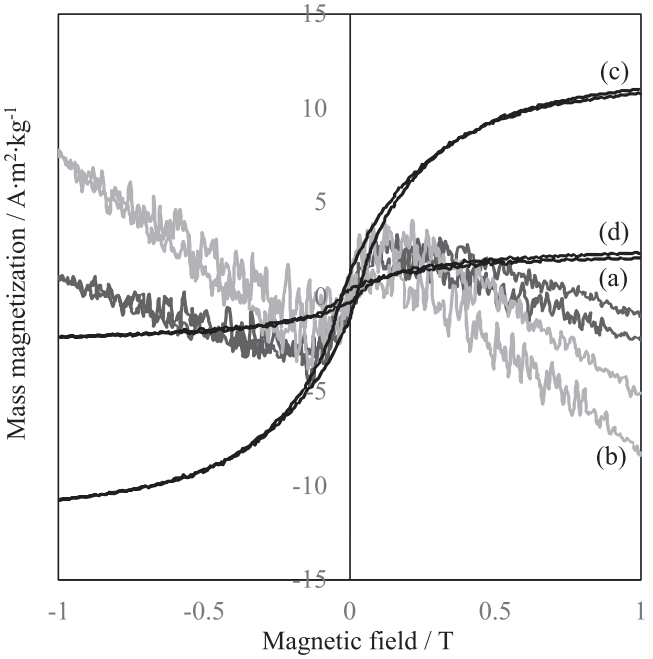

Figure 6. Magnetic hysteresis loop curves for iron oxide films deposited at −0.8 V (a), −0.9 V (b), −1.0 V (c), and −1.1 V (d) vs Ag/AgCl.

$$Fe^{3+} + e^- \rightleftarrows Fe^{2+} \quad [1]$$

$$\Delta_r G^0 = -74.2\ \text{kJ}{\cdot}\text{mol}^{-1}$$
$$NO_3^- + 2H^+ + 2e^- \rightleftarrows NO_2^- + H_2O \quad [2]$$

$$\Delta_r G^0 = 163\ \text{kJ}{\cdot}\text{mol}^{-1},$$
$$E^0 = 0.84\ \text{V (SHE)},\ E = 0.84 - 0.059\ \text{pH} + 0.0295\frac{[NO_3^-]}{[NO_2^-]}\ (\text{V vs SHE})$$
$$Fe^{3+} + 3H_2O \rightleftarrows Fe(OH)_3 + 3H^+ \quad [3]$$

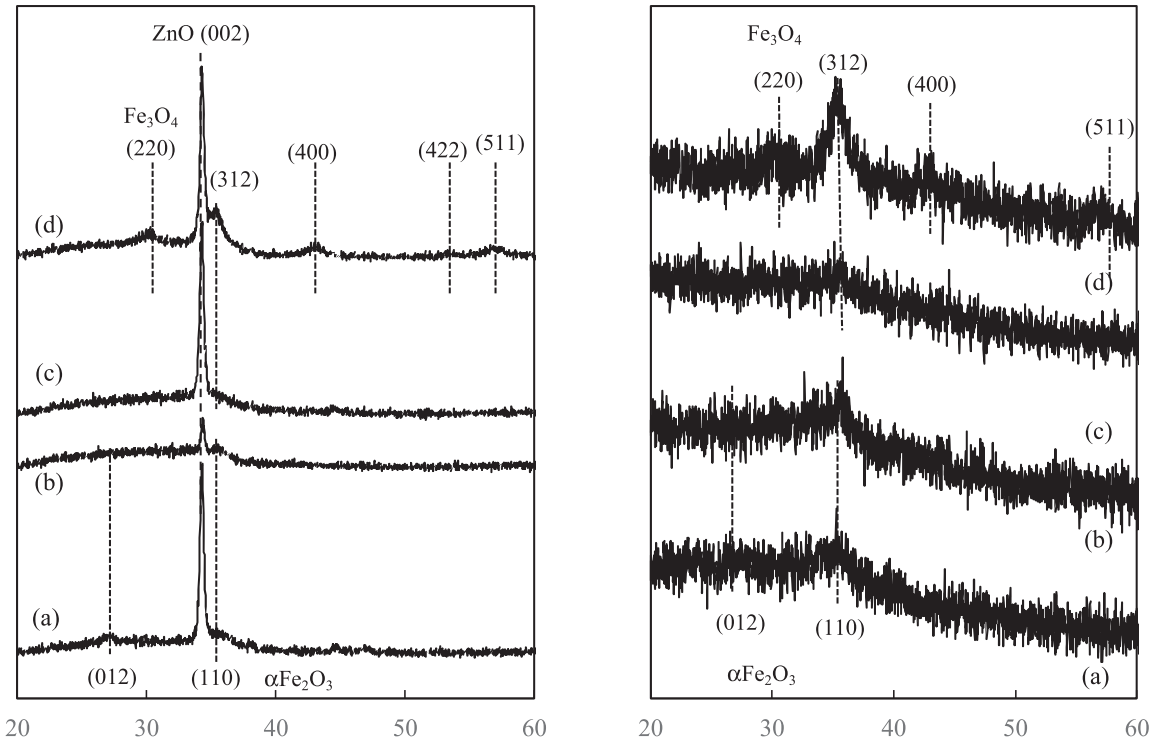

Figure 7. Out-of-plane (A) and GI-X-ray diffraction patterns (B) for hematite films heated at 473 K (a), and 673 K (b) in ambient atmosphere, and 473 K (c), and 673 K (d) in vacuum.

$$\Delta_r G^0 = 19.6\ \text{kJ}\cdot\text{mol}^{-1},$$
$$pH = 1.1 - \frac{1}{3}\log[Fe^{3+}]$$
$$Fe^{2+} + 2H_2O \rightleftarrows Fe(OH)_2 + 2H^+ \qquad [4]$$

$$\Delta_r G^0 = 66.7\ \text{kJ}\cdot\text{mol}^{-1},$$
$$pH = 5.8 - \frac{1}{2}\log[Fe^{2+}]$$

The deposition reaction schemes of magnetite by electrochemical reaction with nitrate reduction reaction was proposed, and according to this, the deposition reaction of the hematite was speculated as follows:

$$2Fe(OH)_3 \rightleftarrows Fe_2O_3 + 3H_2O \qquad [5]$$

$$\Delta_r G^0 = -60.6\ \text{kJ}\cdot\text{mol}^{-1}$$

There were two states of Fe^{2+} and Fe^{3+} in the aqueous solution used for the electrodeposition (reaction 1). The nitrate ions were reduced to nitrite ions by the cathodic polarization at potentials more negative than that of the NO_3^-/NO_2^- reaction (reaction 2). Since the critical pH value for $Fe(OH)_3$ precipitation was lower than that of $Fe(OH)_2$ (reactions 3, 4), $Fe(OH)_3$ can be formed on the cathode substrate, and hematite (α-Fe_2O_3) was formed on the substrate surface due to negative standard Gibbs energy which enabled the progression of Fe_2O_3/$Fe(OH)_3$ reaction (reaction 5).

Effect of heating on the structural and magnetic characteristics of hematite films.—Figure 7 shows the out-of-plane and GI-XRD patterns for the hematite films prepared at −1.0 V after heating at 473 and 673 K in ambient atmosphere and vacuum. The hematite film heated in air showed two peaks assigned to (012) and (110) planes of hematite (α-Fe_2O_3) on both the out-of-plane and GI-XRD patterns. The diffracted X-ray peaks originating from the ZnO in GZO/SLG substrate showed a decrease in intensity on the out-of-plane XRD patterns after heating at 673 K in air. On the other hand, the hematite (110) peaks in the GI-XRD patterns were almost the same in peak angle and intensity irrespective of the heating temperature.

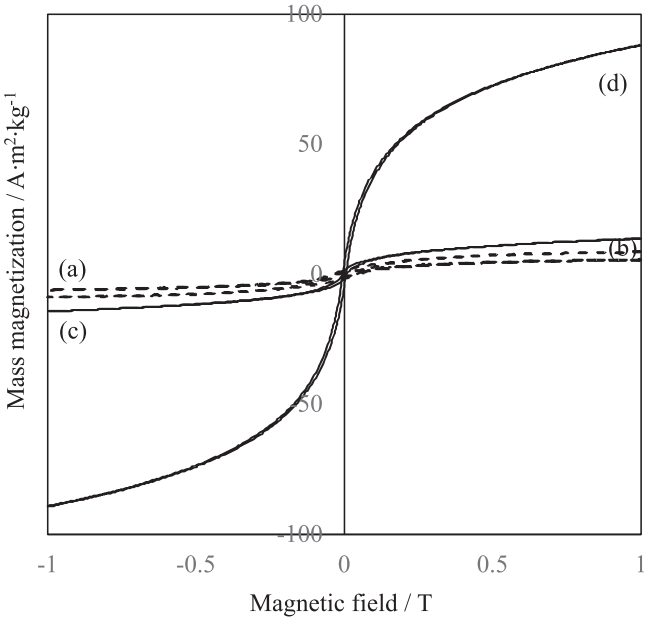

Figure 8. Magnetic hysteresis loop curves for hematite films heated at 473 K (a) and 673 K (b) in ambient atmosphere, and 473 (c) and 673 K (d) in vacuum.

Five diffracted X-ray peaks assigned to the (220), (311), (400), (422), and (511) planes of magnetite (Fe_3O_4) with a characteristic

cubic lattice were observed clearly after heating the hematite film at 673 K in vacuum, along with the disappearance of the (012) hematite peak at around 26 degrees. The lattice constant calculated from the peak angle of the magnetite (311) plane was estimated to be 0.8391 nm, which was close to the standard value of 0.8399 nm.[35] A diffracted X-ray peak was observed at 35.5 degrees after heating at 473 K in air, but the exact peak assignment remained uncertain due to the weak intensity of the peak and the almost similar d-values for magnetite (311) and hematite (110) planes.

Figure 8 shows the magnetic hysteresis curves for the hematite films heated at 473 K and 673 K in ambient atmosphere and vacuum. The saturation mass magnetization increased slightly from 11 $A{\cdot}m^2{\cdot}kg^{-1}$ for the hematite film before heating, to 12.7 and 14 $A{\cdot}m^2{\cdot}kg^{-1}$ after heating at 473 and 673 K in ambient atmosphere, and the coercivities were almost the same at 34 and 30 mT at 473 and 673 K. While the hematite film heated at 473 K in vacuum showed saturation mass magnetization and coercivity at almost the same degree as those before heating, after heating at 673 K in vacuum, there was a drastic increase in saturation mass magnetization to 89.3 $A{\cdot}m^2{\cdot}kg^{-1}$, which was only slightly lower than 92 $A{\cdot}m^2{\cdot}kg^{-1}$ for magnetite.[1] And the coercivity was estimated to be approximately 5 mT. Since the values of the saturation mass magnetization strongly depended on the amount of magnetite, the change in saturation mass magnetization could be attributed to the thermal transformation of hematite to magnetite by heating at 673 K in vacuum by the following reaction:

$$4Fe_3O_4 + O_2 \rightleftarrows 6Fe_2O_3$$

The coercivity for the magnetite film was quite small compared with that already reported for bulk magnetite.[1] Coercivity can be affected by the grain size of the magnetite polycrystalline,[36] suggesting that the small coercivity value measured was attributed to the very small grain size for the magnetite formed by heating, although further investigations on the grain structure are needed.

Conclusions

Hematite (α-Fe_2O_3) films were prepared by cathodic polarization in an aqueous solution containing iron (II) sulfate hydrate, potassium hydroxide, dimethylamine-borane (DMAB), and L-ascorbic acid. The hematite films prepared at −1.0 and −1.1 V possessed characteristic hexagonal lattices and bandgap energies around 2.2 eV, and an increased amount of Fe^{2+} states were contained in the hematite film deposited at −1.0 V. The hematite films prepared at −0.8 and −0.9 V showed characteristic bandgap energies with decreased absorptions but did not show any structural characteristics on XRD and Raman spectra. The hematite films prepared at −1.0 V and −1.1 V showed ferromagnetic features with 11 $A{\cdot}m^2{\cdot}kg^{-1}$ and 2.3 $A{\cdot}m^2{\cdot}kg^{-1}$ in saturation mass magnetization and 29.5 and 25 mT in coercivity, respectively. The hematite film was thermally transformed to magnetite (Fe_3O_4) with a characteristic cubic lattice by heating at 673 K in vacuum, and its saturation mass magnetization increased dramatically to 89.2 $A{\cdot}m^2{\cdot}kg^{-1}$, but its coercivity decreased to 5 mT.

Acknowledgments

This work was supported financially by Grants-in-Aid for Scientific Research (B) (No. 19H02810) from the Japan Society for the Promotion of Science (JSPS).

ORCID

Pei Loon Khoo https://orcid.org/0000-0002-4230-6791
Masakazu Kobayashi https://orcid.org/0000-0002-1906-9097
Tsutomu Shinagawa https://orcid.org/0000-0001-5671-1512
Masanobu Izaki https://orcid.org/0000-0002-3959-1923

References

1. M. Ahmadzadeh, C. Romero, and J. Mccloy, *AIP Adv.*, **8**, 56807 (2018).
2. M. Ojima, F. Shirasaki, Y. Kitamoto, M. Abe, and S. Nagahata, *IEEE Trans. Magn.*, **35**, 4118 (1999).
3. H. G. Cha, C. W. Kim, Y. H. Kim, M. H. Jung, E. S. Ji, B. K. Das, J. C. Kim, and Y. S. Kang, *Thin Solid Films*, **517**, 1853 (2009).
4. M. F. Al-Kuhaili, M. Saleem, and S. M. A. Durrani, *J. Alloys Compd.*, **521**, 178 (2012).
5. F. F. H. Aragón, J. D. Ardisson, J. C. R. Aquino, I. Gonzalez, W. A. A. Macedo, J. A. H. Coaquira, J. Mantilla, S. W. Da Silva, and P. C. Morais, *Thin Solid Films*, **607**, 50 (2016).
6. H. Cui, Y. Liu, and W. Ren, *Adv. Powder Technol.*, **24**, 93 (2013).
7. A. Lassoued, B. Dkhil, A. Gadri, and S. Ammar, *Results Phys.*, **7**, 3007 (2017).
8. M. Izaki and O. Shinoura, *Adv. Mater.*, **13**, 142 (2001).
9. D. Lincot et al., *Sol. Energy*, **77**, 725 (2004).
10. S. Ahmed, K. B. Reuter, O. Gunawan, L. Guo, L. T. Romankiw, and H. Deligianni, *Adv. Energy Mater.*, **2**, 253 (2012).
11. M. Izaki, P. L. Khoo, and T. Shinagawa, *J. Electrochem. Soc.*, **168**, 112510 (2021).
12. M. Izaki and T. Omi, *Appl. Phys. Lett.*, **68**, 2349 (1996).
13. T. D. Golden, M. G. Shumsky, Y. Zhou, R. A. VanderWerf, R. A. Van Leeuwen, and J. A. Switzer, *Chem. Mater.*, **8**, 2499 (1996).
14. M. Izaki, M. Nagai, K. Maeda, F. B. Mohamad, K. Motomura, J. Sasano, T. Shinagawa, and S. Watase, *J. Electrochem. Soc.*, **158**, D578 (2011).
15. M. Izaki, T. Saito, M. Chigane, M. Ishikawa, J. Katayama, M. Inoue, and M. Yamashita, *J. Mater. Chem.*, **11**, 1972 (2001).
16. S. Mitra, P. Poizot, A. Finke, and J. M. Tarascon, *Adv. Funct. Mater.*, **16**, 2281 (2006).
17. T. A. Sorenson, S. A. Morton, G. D. Waddill, and J. A. Switzer, *J. Am. Chem. Soc.*, **124**, 7604 (2002).
18. M. Abe and Y. Tamaura, *J. Appl. Phys.*, **55**, 2614 (1984).
19. M. Izaki, A. Takino, N. Fujita, T. Shinagawa, M. Chigane, S. Ikeda, M. Yamaguchi, K.-I. Arai, and A. Tasaka, *J. Electrochem. Soc.*, **151**, C519 (2004).
20. P. Qiu, F. Li, H. Zhang, S. Wang, Z. Jiang, and Y. Chen, *Electrochim. Acta*, **358**, 136847 (2020).
21. M.-S. Wu, R.-H. Lee, J.-J. Jow, W.-D. Yang, C.-Y. Hsieh, and B.-J. Weng, *Electrochem. Solid-State Lett.*, **12**, A1 (2009).
22. R. Schrebler, K. Bello, F. Vera, P. Cury, E. Muñoz, R. del Río, H. Gómez Meier, R. Córdova, and E. A. Dalchiele, *Electrochem. Solid-State Lett.*, **9**, C110 (2006).
23. M. Schlesinger and M. Paunovic, *Modern Electroplating*, ed. M. Schlesinger and M. Paunovic 5th ed. 309(Wiley, New Jersey, NJ) (2011).
24. M. Pourbaix and J. A. Franklin, *Atlas of Electrochemical Equilibria in Aqueous Solutions* Second. ed.307(National Association of Corrosion Engineers, Houston, Texas, USA) (1974).
25. D. Briggs and M. P. Seah, *Practical Surface Analysis by Auger and X-ray Photoelectron Spectroscopy* (Wiley, Chichester, Sussex, England.) (1984).
26. M. Descostes, F. Mercier, N. Thromat, C. Beaucaire, and M. Gautier-Soyer, *Appl. Surf. Sci.*, **165**, 288 (2000).
27. N. S. McIntyre and D. G. Zetaruk, *Anal. Chem.*, **49**, 1521 (1977).
28. J. F. Moulder, W. F. Stickle, P. E. Sobol, and K. D. Bomben, *Handbook of X-ray Photoelectron Spectroscopy: A Reference Book of Standard Spectra for Identification and Interpretation of Xps Data*J. Chastain, (Perkin-Elmer Corporation, Physical Electronics Division, Eden Prairie, Minnesota, USA.) p. 253 (1992).
29. Joint Committee on Powder Diffraction Standards, *Powder Diffraction File* (International Data for Diffraction Data, Swarthmore, PA) (1992), PDF: 01-076-8397.
30. M. T. De Faria and V. Ncio Silva2 De Oliveira1, *J. Raman Spectrosc.*, **28** (1997).
31. M. Ristić, S. Musić, and M. Godec, *J. Alloys Compd.*, **417**, 292 (2006).
32. E. Darezereshki, *Mater. Lett.*, **65**, 642 (2011).
33. X. Wang and L. Andrews, *J. Phys. Chem. A*, **110**, 10035 (2006).
34. B. Gilbert, C. Frandsen, E. R. Maxey, and D. M. Sherman, *Phys. Rev. B*, **79**, 035108 (2009).
35. Joint Committee on Powder Diffraction Standards, *Powder Diffraction File* (International Data for Diffraction Data, Swarthmore, PA) (1992), PDF: 01-079-0418.
36. G. F. Goya, T. S. Berquó, F. C. Fonseca, and M. P. Morales, *J. Appl. Phys.*, **94**, 3520 (2003).